

Kinetic modeling of CO oxidation over $\text{La}_{1-x}\text{A}_x\text{Mn}_{0.6}\text{Cu}_{0.4}\text{O}_3$ (A = Sr and Ce) nanoperovskite-type mixed oxides

P. R. Zonouz¹ · A. Niaei² · A. Tarjomannejad²

Received: 3 December 2015 / Revised: 10 February 2016 / Accepted: 15 February 2016 / Published online: 11 May 2016
© Islamic Azad University (IAU) 2016

Abstract In this paper, catalytic oxidation of CO over the perovskite-type oxides $\text{La}_{1-x}\text{A}_x\text{Mn}_{0.6}\text{Cu}_{0.4}\text{O}_3$ (A = Sr and Ce, $x = 0, 0.1, 0.2, 0.3$ and 0.4) was investigated. The catalysts were synthesized by sol–gel auto-combustion method and were further characterized by XRD, BET, FT-IR, H_2 -TPR and SEM. XRD patterns revealed that the oxides were single-phase perovskite-type oxides. Traces of Cu_2O_3 , Sr_2O_3 and Ce_2O_3 were also detected in perovskites with high contents of Sr and Ce. Specific surface areas of perovskites were also determined to be about 16 and $32 \text{ m}^2/\text{g}$. Reducibility of the perovskites, also, is strongly affected by substitution of La in A site by Sr and Ce. Perovskite catalysts show a high activity in catalytic oxidation of CO; substitution of Sr and Ce further enhanced CO oxidation activity. Highest activity was achieved by $\text{La}_{0.7}\text{Ce}_{0.3}\text{Mn}_{0.6}\text{Cu}_{0.4}\text{O}_3$: Nearly complete elimination of CO was achieved at $145 \text{ }^\circ\text{C}$ with this catalyst. Kinetic studies for CO oxidation were performed based on Langmuir–Hinshelwood mechanisms. According to kinetic calculations, the most probable mechanism is the LH–OS–ND (adsorption of the reagents on same types of sites and non-dissociative adsorption of oxygen) which can predict the experimental data with correlation coefficient of $R^2 = 0.9933$.

Keywords $\text{La}_{1-x}\text{A}_x\text{Mn}_{0.6}\text{Cu}_{0.4}\text{O}_3$ · Perovskite · CO oxidation · Kinetic

✉ A. Niaei
aniaei@tabrizu.ac.ir

¹ Faculty of Engineering, Tehran North Branch, Islamic Azad University, Tehran, Iran

² Department of Chemical Engineering and Petroleum, University of Tabriz, 29 Bahman Blv., Tabriz, Iran

Introduction

Carbon monoxide (CO), one of the main air pollutants, is generally released by the combustion of fossil fuels in diesel engines (Jaenicke et al. 1991). Several techniques have been used for removal of waste materials among which include supported metal (Ferrer et al. 2015; Piccolo et al. 1999), activated carbon (Gupta et al. 2011a, c), particulate filters (Wagloehner et al. 2008), perovskite and spinel mixed oxides (Singh et al. 2007; Yoon et al. 2014). Catalytic oxidation of the diesel exhaust CO gas is proved to be one of the most efficient techniques to remove this pollutant (Ladas et al. 1981; Xu et al. 1994).

Present catalysts, supported noble metal catalysts based on platinum, palladium, and rhodium, suffer from high cost, low stability and lack of noble metals (Libby 1971; Voorhoeve et al. 1977). Perovskite-type oxides are interesting catalysts for CO oxidation (Pena and Fierro 2001; Singh et al. 2007; Yoon et al. 2014).

Perovskite-type oxides have been investigated extensively due to their physical and catalytic properties, cheaper price and higher thermal stability (Khanfekr et al. 2009). Perovskite oxides general formula is ABO_3 where ‘A’ cation surrounded by six oxygen ions in the cubic structure, and oxygen ions are occupied by the small ‘B’ cations. ‘A’ cations can be rare earth elements or base metals such as lanthanum, barium, cerium and strontium, while ‘B’ cations are usually transition metals (Khanfekr et al. 2009; Yan et al. 2013). Both ‘A’ and ‘B’ cations can be partially substituted, leading to formation of substituted compounds with a general formula of $\text{A}_{1-x}\text{A}'_x\text{B}_{1-y}\text{B}'_y\text{O}_3$.

Perovskites with La in ‘A’ site and manganese or copper in ‘B’ site show high activation for oxidation of CO (Gao et al. 2013; Yan et al. 2013). La can be partially substituted by other ions such as Sr and Ce (Patel and Patel 2013;

Wang and Zhong 2010). Substitution of La^{3+} by Sr^{2+} leads to partial reduction of Mn^{3+} to Mn^{4+} . Substitution of La^{3+} by Ce^{4+} leads to partial reduction of Mn^{3+} of Mn^{2+} .

To investigate the effect of partial substitution of 'A' site, $\text{La}_{1-x}\text{A}_x\text{Mn}_{0.6}\text{Cu}_{0.4}\text{O}_3$ ($\text{A} = \text{Sr}$ and Ce , $x = 0, 0.1, 0.2, 0.3$ and 0.4) perovskite catalysts were synthesized by sol–gel auto-combustion method and then catalytic activity of these catalysts for CO oxidation was measured. Perovskites were characterized using XRD, BET, FT-IR, H_2 -TPR and SEM. To investigate the kinetics of CO oxidation reaction, kinetic studies were conducted based on Langmuir–Hinshelwood mechanisms, and the rate constant and activation energy were evaluated under specified operating condition.

This work was carried out in catalyst laboratory of Department of Chemical Engineering and Petroleum, University of Tabriz, Tabriz, Iran, 2015.

Materials and methods

Materials

$\text{La}(\text{NO}_3)_3 \cdot 6\text{H}_2\text{O}$, $\text{Sr}(\text{NO}_3)_2$, $\text{Ce}(\text{NO}_3)_3$ were all obtained from Sigma–Aldrich with purity of 99.0 %. Other materials including $\text{Cu}(\text{NO}_3)_2 \cdot 3\text{H}_2\text{O}$, $\text{Mn}(\text{NO}_3)_2 \cdot 3\text{H}_2\text{O}$ and citric acid were obtained from Merck with purity of 99.9 %. All chemicals were of analytical grade.

Catalyst preparation

The perovskite-type oxide powders with general formulas of $\text{La}_{1-x}\text{Sr}_x\text{Mn}_{0.6}\text{Cu}_{0.4}\text{O}_3$ and $\text{La}_{1-x}\text{Ce}_x\text{Mn}_{0.6}\text{Cu}_{0.4}\text{O}_3$ ($x = 0.0, 0.1, 0.2, 0.3$ and 0.4) were prepared by sol–gel auto-combustion method. $\text{La}(\text{NO}_3)_3 \cdot 6\text{H}_2\text{O}$, $\text{Sr}(\text{NO}_3)_2$, $\text{Ce}(\text{NO}_3)_3$, $\text{Cu}(\text{NO}_3)_2 \cdot 3\text{H}_2\text{O}$, $\text{Mn}(\text{NO}_3)_2 \cdot 3\text{H}_2\text{O}$ and citric acid were used as the starting materials. For preparation of 1 g of catalyst, appropriate amount of La, A, Mn and Cu nitrates with cation ratios of La:A:Mn:Cu, of $1 - x:x:0.6:0.4$ were dissolved in 50 ml of deionized water. The solution was stirred and heated on a hot plate, and when the temperature of the solution was raised to 70 °C, citric acid was added to the solution, while molar ratio of citric acid to the total nitrates in the solution mixture was kept at 0.525. Water was evaporated under slow stirring of the mixed solution at 80 °C until a viscous gel was obtained. In order to carry out gel decomposition, temperature was raised to 200 °C, and finally the decomposed gel self-ignited and turned into a dark powder. Then, the powder was calcined for 5 h at 700 °C.

Catalyst characterization

Identification of crystal structure of perovskites was carried out using X-ray diffractometer (D-500, SIEMENS) with a

$\text{Cu K}\alpha$ line ($\lambda = 0.154$ nm). Diffractograms were recorded with a step of 4° per minute for 2θ between 20° and 80°. Specific surface area (BET) of perovskites was determined from nitrogen adsorption isotherm in the relative pressure (p/p_0) between 0.05 and 0.30 obtained at 77.35 K using Autosorb-1 Quantachrome analyzer.

FT-IR spectra were recorded using a Bruker spectrometer (model TENSOR 27, USA) using the Universal ATR Accessory in the range from 4000 to 400 cm^{-1} . For FT-IR spectroscopy, samples were pressed into self-supporting wafers of 10–15 mg cm^{-2} surface density and placed into a glass cell sealed by KBr windows.

Temperature-programmed reduction (TPR) measurements were taken with Micromeritics Autochem 2900 (USA). Samples were pre-treated with a gaseous mixture containing 5 vol% oxygen in helium at 500 °C for 2 h. Hydrogen consumption was measured with a mixture of 5 vol% H_2 in argon at 20 cm^3/min and a linear heating rate of 10 °C/min at 40–950 °C. The size and morphology of perovskites were observed by scanning electron microscopy (FESEM, Tescan, Czech Republic).

Catalytic activity

Catalytic activity tests for CO oxidation were performed using a conventional fixed bed reactor (i.d. 9 mm) under atmospheric pressure. In a typical experiment, the reactant gas composition was as follows: 1 % CO, 20 % O_2 and argon as balance. For evaluating the activity of catalysts, 200 mg of synthesized powder, under a flow rate of adjusted to 100 ml/min, was used. An electrical furnace was used to evaluate the reaction temperature from 55 to 210 °C.

The catalytic reactions were performed under steady-state conditions in which all process variables remained constant with time at any given point in the reactor before any measurement was taken. CO concentrations in inlet and outlet of system were analyzed online by a gas chromatograph (Shimadzu 2010) equipped with a TCD detector and an HP-Molesieve (Agilent, USA) column ($l = 30$ m, i.d. = 0.53 mm).

Results and discussion

Characterization

XRD patterns of $\text{La}_{1-x}\text{Sr}_x\text{Mn}_{0.6}\text{Cu}_{0.4}\text{O}_3$ and $\text{La}_{1-x}\text{Ce}_x\text{Mn}_{0.6}\text{Cu}_{0.4}\text{O}_3$ ($x = 0, 0.2, 0.3$ and 0.4) are shown in Fig. 1. Comparison to standard patterns reveals that XRD patterns of catalysts are compatible with standard patterns of LaCuO_3 (01-071-0872.CAF) and LaMnO_3 (01-086-1226.CAF). In high content of Sr and Ce, traces of Cu_2O_3 ,

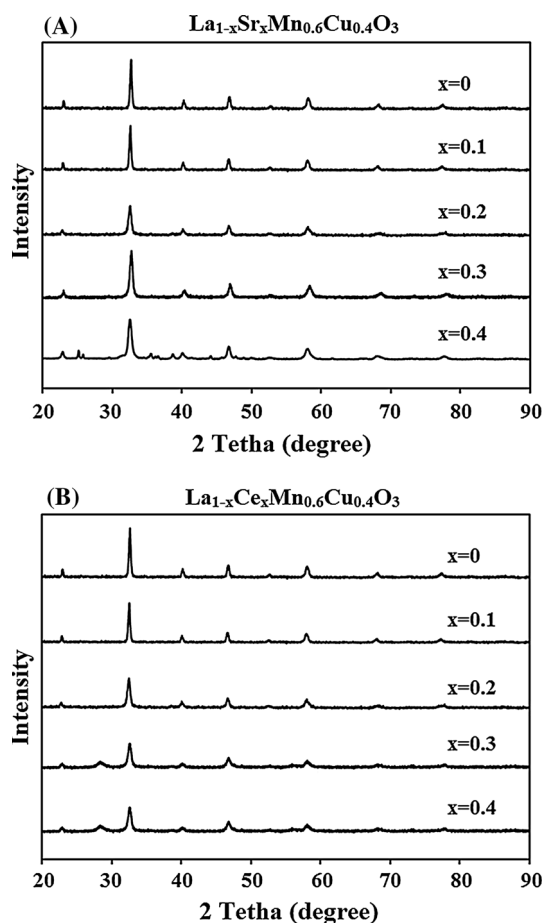


Fig. 1 X-ray patterns of $\text{La}_{1-x}\text{A}_x\text{Mn}_{0.6}\text{Cu}_{0.4}\text{O}_3$ perovskites: **a** $\text{La}_{1-x}\text{Sr}_x\text{Mn}_{0.6}\text{Cu}_{0.4}\text{O}_3$ and **b** $\text{La}_{1-x}\text{Ce}_x\text{Mn}_{0.6}\text{Cu}_{0.4}\text{O}_3$

Sr_2O_3 and Ce_2O_3 were also detected in the catalyst. By substituting Sr and Ce, diffraction lines of this structure were being broadened slightly.

The ionic radii of Sr^{2+} (0.118 nm) and Ce^{3+} (0.101 nm) are close to La^{3+} (0.103 nm) ion; therefore, the doping of these cations into $\text{LaMn}_{0.6}\text{Cu}_{0.4}\text{O}_3$ perovskite structure is expected (Meiqing et al. 2013). Mean crystallite size of synthesized catalysts was calculated by Scherrer equation ($D = K\lambda/\beta \cos \theta$). Results show that mean crystallite size is in the range of 21–35 nm.

Specific surface areas of perovskites are listed in Table 1 which varies between 16 and 32 m^2/g . Results show that the specific surface area of $\text{La}_{1-x}\text{A}_x\text{Mn}_{0.6}\text{Cu}_{0.4}\text{O}_3$ catalysts decreased in comparison with specific surface area of $\text{LaMn}_{0.6}\text{Cu}_{0.4}\text{O}_3$. Most reduction was observed in the case of $\text{La}_{0.7}\text{Sr}_{0.3}\text{Mn}_{0.6}\text{Cu}_{0.4}\text{O}_3$.

Figure 2 shows the FT-IR spectra of perovskites in the range of 400–4000 cm^{-1} . The broad absorption peaks at 3448 cm^{-1} can be attributed to either the hydroxyl groups on the surface of the perovskite or the adsorption of some atmospheric water during FT-IR experiments (Gupta et al.

Table 1 Specific surface area of perovskites

Catalyst number	Catalyst	Surface area (m^2/g)
1	$\text{LaMn}_{0.6}\text{Cu}_{0.4}\text{O}_3$	32
2	$\text{La}_{0.8}\text{Sr}_{0.2}\text{Mn}_{0.6}\text{Cu}_{0.4}\text{O}_3$	19
3	$\text{La}_{0.7}\text{Sr}_{0.3}\text{Mn}_{0.6}\text{Cu}_{0.4}\text{O}_3$	16
4	$\text{La}_{0.8}\text{Ce}_{0.2}\text{Mn}_{0.6}\text{Cu}_{0.4}\text{O}_3$	18
5	$\text{La}_{0.7}\text{Ce}_{0.3}\text{Mn}_{0.6}\text{Cu}_{0.4}\text{O}_3$	17

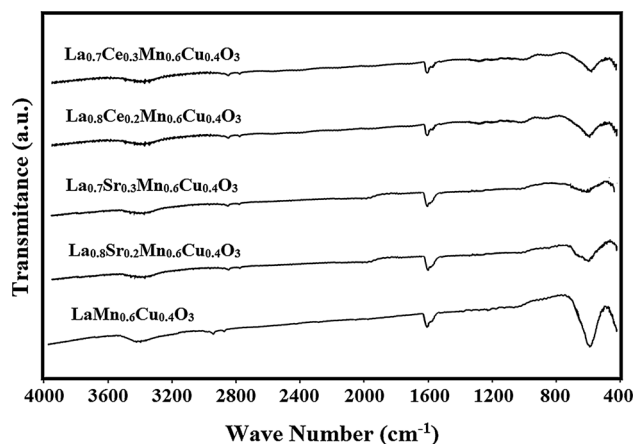


Fig. 2 FT-IR spectra of perovskite catalysts in the range of 400–4000 cm^{-1}

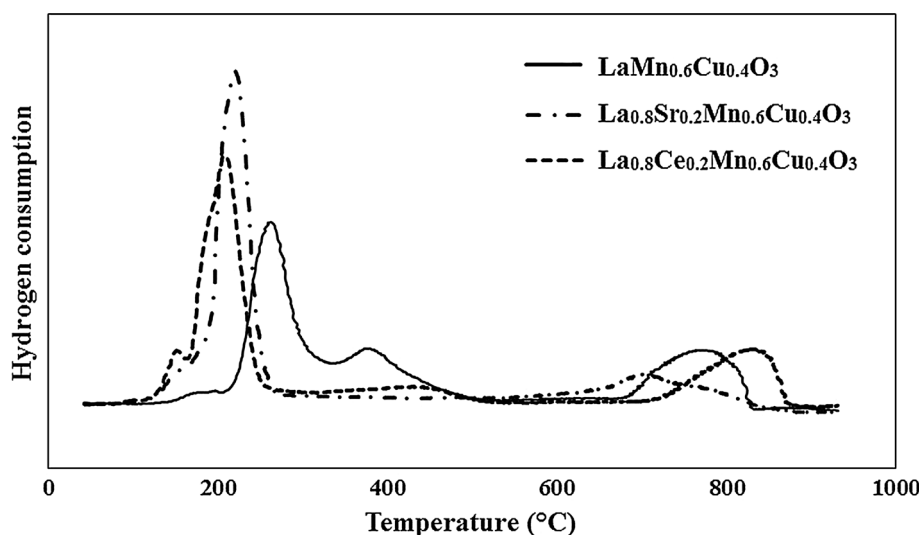
2011c; Hosseini et al. 2010). The peak around 2920 cm^{-1} represents asymmetric and symmetric stretching of CH and indicates the presence of aliphatic $-\text{CH}_2$ groups (Saleh 2016). The peak around 1640 cm^{-1} is assigned to asymmetric C=O band in carboxyl or acid ($-\text{COOH}$) groups (Megha et al. 2014; Saleh et al. 2011). Bands around 600–400 cm^{-1} are characteristic metal–oxygen bond (Hosseini et al. 2013; Saleh and Gupta 2012). These bands are assigned for Mn–O and Cu–O bonds (Saleh et al. 2011).

H_2 -TPR experiments were also conducted to study the effects of partial substitution of Sr and Ce ions on the reducibility of perovskites. H_2 -TPR curves of the perovskites are shown in Fig. 3. TPR results of $\text{LaMn}_{0.6}\text{Cu}_{0.4}\text{O}_3$ showed three significant reduction peaks at 260, 380 and 780 $^\circ\text{C}$. The first peak can be assigned to reduction of Cu^{2+} to Cu^0 . The second peak corresponds to Mn^{4+} reduction to Mn^{3+} , and the third peak represented the reduction of Mn^{3+} to Mn^{2+} (Abdollahmani et al. 2010; Hosseini et al. 2013; Meiqing et al. 2013). In the TPR profiles of $\text{La}_{0.8}\text{Sr}_{0.2}\text{Mn}_{0.6}\text{Cu}_{0.4}\text{O}_3$ and $\text{La}_{0.8}\text{Ce}_{0.2}\text{Mn}_{0.6}\text{Cu}_{0.4}\text{O}_3$, overlapping of first and second peaks can be attributed to reduction of Cu^{2+} to Cu^0 and Mn^{4+} to Mn^{3+} .

Evidently, the doping of Sr decreased the intensity of the Mn³⁺ reduction peak, indicating the higher content of



Fig. 3 H₂-TPR profile of perovskites, 5 % H₂/Ar gas flow at 20 sccm, linear heating rate of 10 °C/min



Mn⁴⁺; however, introduction of Ce increased the intensity of the Mn³⁺ reduction peak indicating the lower content of Mn⁴⁺. With introduction of both ions, the reduction peak of Cu²⁺ shifted toward lower temperature. Based on these results, doping of strontium and cerium leads to decreased reduction temperatures for samples and an increased hydrogen consumption during reduction. Therefore, reduction ability of catalysts was increased by doping strontium and cerium to the perovskite structure.

Morphology and particle size of perovskites were investigated by scanning electron microscopy. Figure 4 illustrates the SEM micrographs of samples. It is observed that the particle sizes are different for the samples. Results show that the crystals size is less than 100 nm. Particles were spherical; La substitution by Sr and Ce led to change of surface structure and reduced the size of crystals.

Catalyst activity

Results of catalytic activity tests over oxidation of carbon monoxide for La_{1-x}Sr_xMn_{0.6}Cu_{0.4}O₃ and La_{1-x}Ce_xMn_{0.6}Cu_{0.4}O₃ are shown in Fig. 5. Temperatures for 50 % conversion of CO (T50 %) on La_{1-x}Sr_xMn_{0.6}Cu_{0.4}O₃ and La_{1-x}Ce_x hydrogen Mn_{0.6}Cu_{0.4}O₃ are given in Table 2. Considering the T50 % of CO conversion as criterion of activity, La_{0.7}Ce_{0.3}Mn_{0.6}Cu_{0.4}O₃ is the most active catalyst for CO oxidation as 100 % of CO combustion can be achieved only at 160 °C. Obviously, partial substitution of Ce and Sr in A site has a significant effect on the catalyst activity. However, no direct relationship was observed between activity and specific surface area of perovskites.

Oxidation of CO depends on the reducibility of the transition metal cations. Introduction of Sr²⁺ and Ce⁴⁺ in A site of perovskite changed the reducibility of cations in B site and the ratio of Mn⁴⁺/Mn³⁺ which can cause structural defects in

perovskite structure (Tanaka and Misono 2001). More structural defects and oxygen vacancies lead to higher catalytic activity and improve perovskite performance (Lin and Hohn 2014). The enhancement in catalytic performance can be explained based on oxygen adsorption (Saleh and Gupta 2011). By introducing Sr²⁺ and Ce⁴⁺ ions into the ‘A’ site of perovskite, metal ions of ‘B’ cations can get abnormal valences. These ions tend to be reduced by releasing α -oxygen from the lattice of perovskite.

Kinetic modeling

Kinetic modeling based on adsorption isotherms is useful in describing how catalysts interrelate with the reactants, hence critical in optimizing implementing the catalysts (Gupta et al 2011b; Karthikeyan et al. 2012). Langmuir isotherms were used to analyze the adsorption isotherm results which have been successfully applied in the kinetic modeling of real processes (Gupta et al. 2011d, 2012).

Four Langmuir–Hinshelwood models have been developed for CO oxidation (Harriott 2002; Vannice and Joyce 2005). Based on Langmuir–Hinshelwood models, reaction rate can be expressed by Eq. (1):

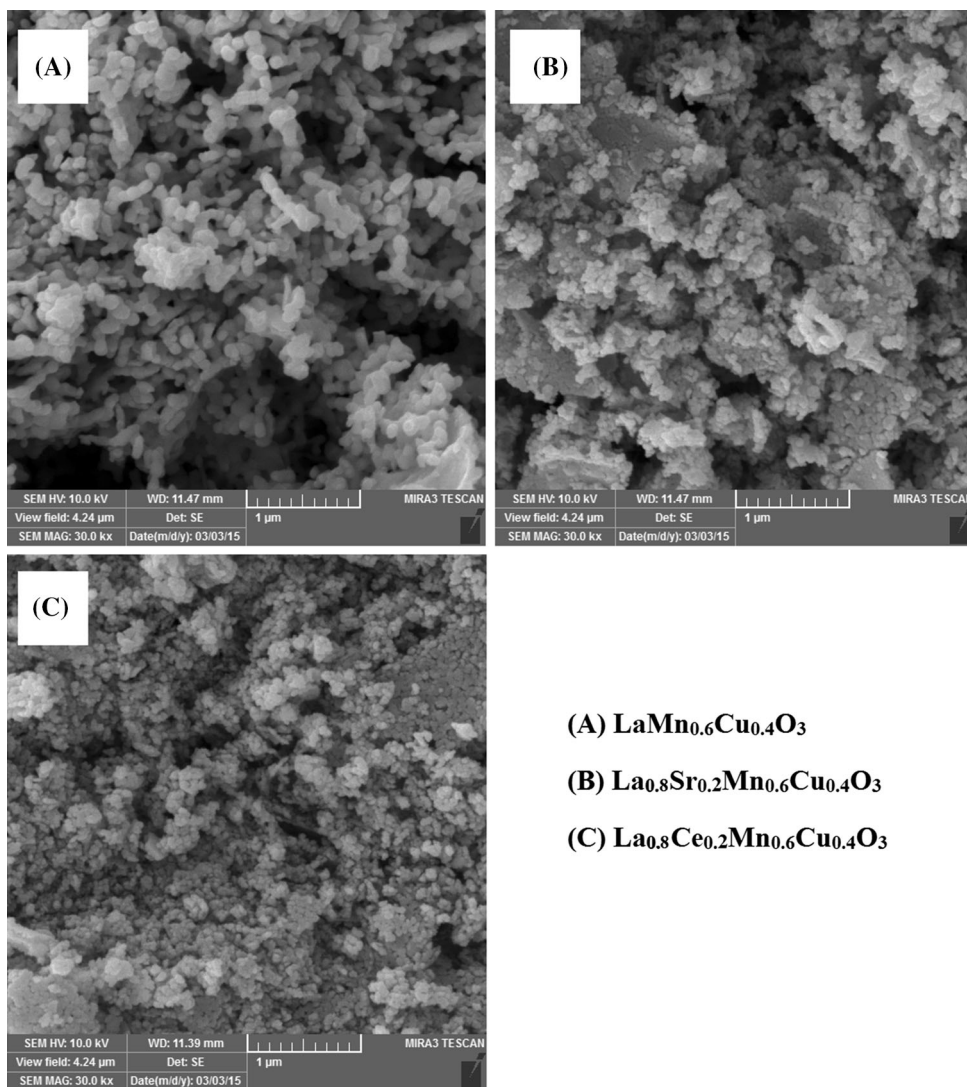
$$r = k\theta_{\text{CO}}\theta_{\text{OX}} \quad (1)$$

where θ is the corresponding surface coverage derived on the basis of Langmuir’s isotherm.

LH–OS–ND: First LH models hypothesized the existence of competitive adsorption on one single type of sites and non-dissociative adsorption of oxygen (LH–OS–ND). In this case, reaction steps have to be formulated based on Eqs. (2) and (3).



Fig. 4 SEM image of
a $\text{LaMn}_{0.6}\text{Cu}_{0.4}\text{O}_3$,
b $\text{La}_{0.8}\text{Sr}_{0.2}\text{Mn}_{0.6}\text{Cu}_{0.4}\text{O}_3$ and
c $\text{La}_{0.8}\text{Ce}_{0.2}\text{Mn}_{0.6}\text{Cu}_{0.4}\text{O}_3$



(A) $\text{LaMn}_{0.6}\text{Cu}_{0.4}\text{O}_3$
(B) $\text{La}_{0.8}\text{Sr}_{0.2}\text{Mn}_{0.6}\text{Cu}_{0.4}\text{O}_3$
(C) $\text{La}_{0.8}\text{Ce}_{0.2}\text{Mn}_{0.6}\text{Cu}_{0.4}\text{O}_3$

where S is a surface active site. Based on Eqs. (2) and (3), expressions of the fractions of occupied sites can be derived as follows:

$$r_{\text{CO,ads}} = k_{1\text{CO}}P_{\text{CO}}(1 - \theta) = k_{1\text{CO}}P_{\text{CO}}(1 - \theta_{\text{CO}} - \theta_{\text{OX}}) \tag{4}$$

$$r_{\text{CO,des}} = K_{2\text{CO}}\theta_{\text{CO}} \tag{5}$$

$$r_{\text{OX,ads}} = k_{1\text{OX}}P_{\text{OX}}(1 - \theta) = k_{1\text{OX}}P_{\text{OX}}(1 - \theta_{\text{CO}} - \theta_{\text{OX}}) \tag{6}$$

$$r_{\text{OX,des}} = K_{2\text{OX}}\theta_{\text{OX}} \tag{7}$$

Substituting $\frac{k_{1\text{CO}}}{k_{2\text{CO}}}$ and $\frac{k_{1\text{O}}}{k_{2\text{O}}}$ with K_{CO} and K_{O} gives:

$$\theta_{\text{CO}} = \frac{K_{\text{CO}}P_{\text{CO}}}{1 + K_{\text{CO}}P_{\text{CO}} + K_{\text{OX}}P_{\text{OX}}} \tag{8}$$

$$\theta_{\text{OX}} = \frac{K_{\text{OX}}P_{\text{OX}}}{1 + K_{\text{CO}}P_{\text{CO}} + K_{\text{OX}}P_{\text{OX}}} \tag{9}$$

$$r = k \frac{K_{\text{CO}}P_{\text{CO}}K_{\text{OX}}P_{\text{OX}}}{(1 + K_{\text{CO}}P_{\text{CO}} + K_{\text{OX}}P_{\text{OX}})^2} \tag{10}$$

LH–OS–D: Second LH model hypothesized the existence of competitive adsorption on one single type of sites and dissociative adsorption of oxygen (LH–OS–D). In this case, reaction steps are based on Eqs. (11) and (12) and the rate equations will be derived as Eqs. (13)–(15).



$$\theta_{\text{CO}} = \frac{K_{\text{CO}}P_{\text{CO}}}{1 + K_{\text{CO}}P_{\text{CO}} + K_{\text{OX}}^{\frac{1}{2}}P_{\text{OX}}^{\frac{1}{2}}} \tag{13}$$

$$\theta_{\text{OX}} = \frac{K_{\text{OX}}^{\frac{1}{2}}P_{\text{OX}}^{\frac{1}{2}}}{1 + K_{\text{CO}}P_{\text{CO}} + K_{\text{OX}}^{\frac{1}{2}}P_{\text{OX}}^{\frac{1}{2}}} \tag{14}$$

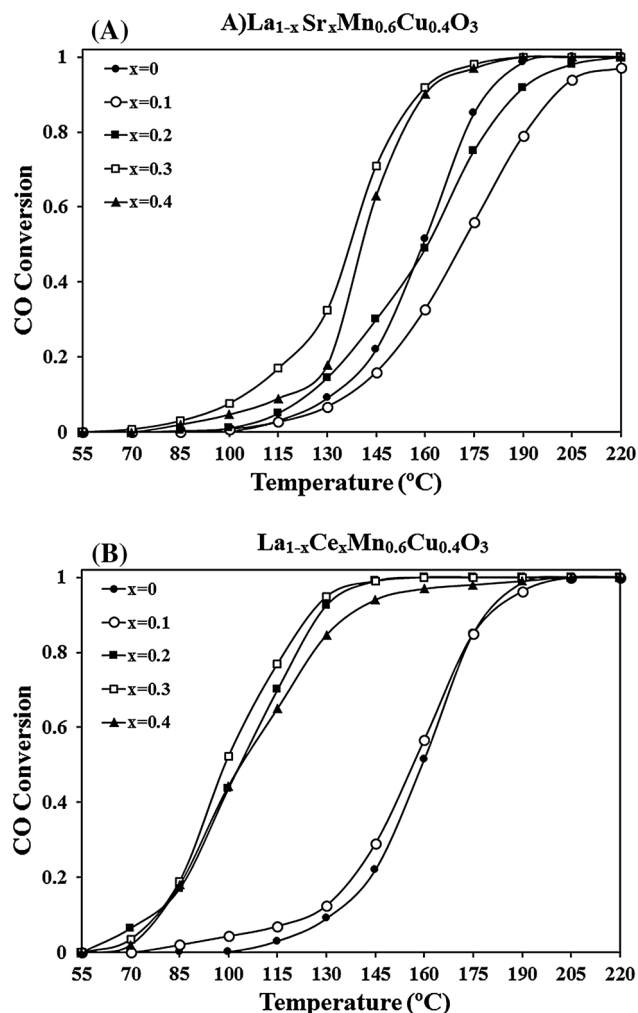


Fig. 5 Temperature profiles for CO conversion, catalyst 200 mg, gas flow rate 200 cm³/min, reaction gas composition NO (3000 ppm)–CO (3000 ppm)–Ar (balance). La_{1-x}A_xMn_{0.6}Cu_{0.4}O₃ catalysts: **a** La_{1-x}Sr_xMn_{0.6}Cu_{0.4}O₃ and **b** La_{1-x}Ce_xMn_{0.6}Cu_{0.4}O₃

Table 2 T50% on La_{1-x}A_xMn_{0.6}Cu_{0.4}O₃

Catalyst	T50% (°C)
LaMn _{0.6} Cu _{0.4} O ₃	159
La _{0.9} Sr _{0.1} Mn _{0.6} Cu _{0.4} O ₃	172
La _{0.8} Sr _{0.2} Mn _{0.6} Cu _{0.4} O ₃	161
La _{0.7} Sr _{0.3} Mn _{0.6} Cu _{0.4} O ₃	137
La _{0.6} Sr _{0.4} Mn _{0.6} Cu _{0.4} O ₃	141
La _{0.9} Ce _{0.1} Mn _{0.6} Cu _{0.4} O ₃	156
La _{0.8} Ce _{0.2} Mn _{0.6} Cu _{0.4} O ₃	103
La _{0.7} Ce _{0.3} Mn _{0.6} Cu _{0.4} O ₃	98
La _{0.6} Ce _{0.4} Mn _{0.6} Cu _{0.4} O ₃	103

$$r = k \frac{K_{CO}P_{CO}K_{OX}^{\frac{1}{2}}P_{OX}^{\frac{1}{2}}}{\left(1 + K_{CO}P_{CO} + K_{OX}^{\frac{1}{2}}P_{OX}^{\frac{1}{2}}\right)^2} \quad (15)$$

LH–DS–ND: Third LH model hypothesized the existence of adsorption on different sites and non-dissociative adsorption of oxygen (LH–DS–ND). In this case, reaction steps are based on Eqs. (16) and (18) and the rate equations obtained according to Eqs. (19)–(21).



$$\theta_{CO} = \frac{K_{CO}P_{CO}}{1 + K_{CO}P_{CO}} \quad (19)$$

$$\theta_{OX} = \frac{K_{OX}P_{OX}}{1 + K_{OX}P_{OX}} \quad (20)$$

$$r = k \frac{K_{CO}P_{CO}K_{OX}P_{OX}}{\left(1 + K_{CO}P_{CO}\right)\left(1 + K_{OX}P_{OX}\right)} \quad (21)$$

LH–DS–ND: Fourth LH model hypothesized the existence of adsorption on different sites and non-dissociative adsorption of oxygen (LH–DS–ND). In this case, reaction steps are based on Eqs. (22)–(24) and the rate equations can be derived according to Eqs. (25)–(27).



$$\theta_{CO} = \frac{K_{CO}P_{CO}}{1 + K_{CO}P_{CO}} \quad (25)$$

$$\theta_{OX} = \frac{K_{OX}^{\frac{1}{2}}P_{OX}^{\frac{1}{2}}}{1 + K_{OX}^{\frac{1}{2}}P_{OX}^{\frac{1}{2}}} \quad (26)$$

$$r = k \frac{K_{CO}P_{CO}K_{OX}^{\frac{1}{2}}P_{OX}^{\frac{1}{2}}}{\left(1 + K_{CO}P_{CO}\right)\left(1 + K_{OX}^{\frac{1}{2}}P_{OX}^{\frac{1}{2}}\right)} \quad (27)$$

k_1 , K_{CO} and K_{OX} are expressed as Eqs. (28)–(30), respectively:

$$k_1 = k_0 \exp\left(\frac{-E_1}{RT}\right) \quad (28)$$

$$K_{CO} = k_{0,CO} \exp\left(\frac{\Delta H_{CO}}{RT}\right) \quad (29)$$

$$K_{OX} = K_{0,OX} \exp\left(\frac{\Delta H_{OX}}{RT}\right) \quad (30)$$

Table 3 R^2 and AAD% for various model and estimated parameters according to the fitting of catalytic data for LH–OS–ND model

Model	LH–DS–ND	LH–DS–D	LH–OS–ND	LH–OS–D
AAAD%	2.5936	3.7405	2.2096	2.8036
R^2	0.9887	0.9774	0.9933	0.9836

LH–OS–ND model								
Catalyst	k_0	$k_{0,CO}$	$k_{0,OX}$	E_1 (j/mol)	ΔH_{CO} (j/mol)	ΔH_{ox} (j/mol)	R^2	AAAD%
LaMn _{0.6} Cu _{0.4} O ₃	1.98E+09	1.76E–03	4.14E–06	28,498.02	–89,700.1	–57,551.4	0.9945	2.361
La _{0.9} Sr _{0.1} Mn _{0.6} Cu _{0.4} O ₃	1.30E+10	9.11E–02	5.32E–06	23,498.02	–95,700.1	–63,551.4	0.9929	2.429
La _{0.8} Sr _{0.2} Mn _{0.6} Cu _{0.4} O ₃	5.14E+09	2.11E–02	4.12E–06	27,841.02	–88700.1	–61551.4	0.9941	2.294
La _{0.7} Sr _{0.3} Mn _{0.6} Cu _{0.4} O ₃	1.51E+10	6.11E–03	2.99E–06	31,841.02	–82,700.1	–55,551.4	0.9939	1.799
La _{0.6} Sr _{0.4} Mn _{0.6} Cu _{0.4} O ₃	1.30E+10	1.11E–02	4.44E–06	30,504.02	–84,700.1	–56,551.4	0.9946	2.244
La _{0.9} Ce _{0.1} Mn _{0.6} Cu _{0.4} O ₃	2.43E+09	1.56E–03	3.32E–06	28,902.02	–89,581.1	–58,051.4	0.9952	1.726
La _{0.8} Ce _{0.2} Mn _{0.6} Cu _{0.4} O ₃	1.24E+10	2.48E–03	4.24E–06	33,020.85	–78,055.3	–53,392.1	0.9922	1.964
La _{0.7} Ce _{0.3} Mn _{0.6} Cu _{0.4} O ₃	2.46E+10	2.18E–03	5.18E–06	33,616.85	–79,055.3	–52,392.1	0.9908	2.255
La _{0.6} Ce _{0.4} Mn _{0.6} Cu _{0.4} O ₃	1.04E+11	1.10E–02	4.21E–06	32,841.02	–877,00.1	–60,551.4	0.9923	2.812

The catalytic bed, which has been modeled as a one-dimensional system, is treated as a plug flow reactor. The mass balance equations at steady-state condition are according to Eq. (18).

$$\frac{dc_i}{dz} = \frac{1}{u_{eff}} \sum_j v_j r_j \quad i = \text{VOC and O}_2 \quad (31)$$

For fitting the kinetic parameters, continuity equations for toluene and oxygen in steady-state condition are solved numerically. These simulations were created by writing computer codes in MATLAB™ 7.2 software. A nonlinear least square algorithm minimizes average absolute derivation between the experimental and calculated data. The average absolute deviation percent AAAD% and correlation coefficient R^2 were used to evaluate the accuracy of models (Tarjomannejad 2015).

$$AAAD\% = \frac{1}{N} \sum_{i=1}^N 100 \times |X_i^{exp} - X_i^{cal}| \quad (32)$$

$$R^2 = \frac{\sum_{i=1}^N (X_i^{exp} - \bar{X})^2 - \sum_{i=1}^N (X_i^{exp} - X_i^{cal})^2}{\sum_{i=1}^N (X_i^{exp} - \bar{X})^2} \quad (33)$$

where N is the number of experimental data points; X_i^{exp} is the i th experimental value; X_i^{cal} is the i th predicted value with ANN model; \bar{X} is the average value of experimental data.

The correlation coefficients (R^2) and average absolute derivation (AAAD%) for various models are listed in Table 3. These parameters are calculated based on differences between experimental and calculated data for each catalyst. Results show that LH–OS–ND model can best describe the behavior of catalysts, while other models are not satisfactory considering the experimental results. The

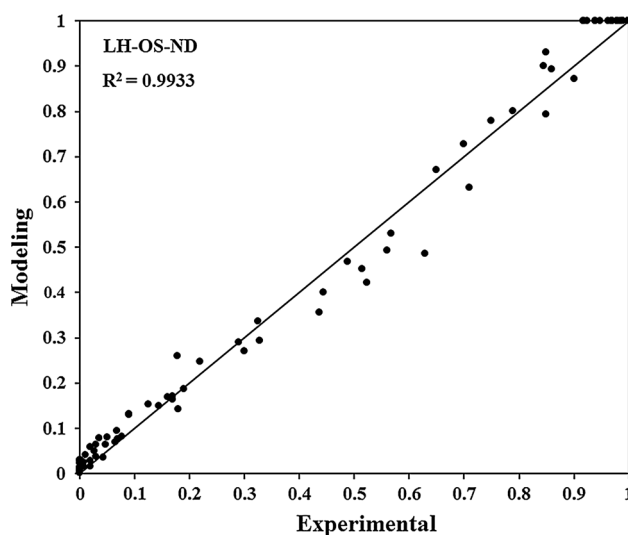
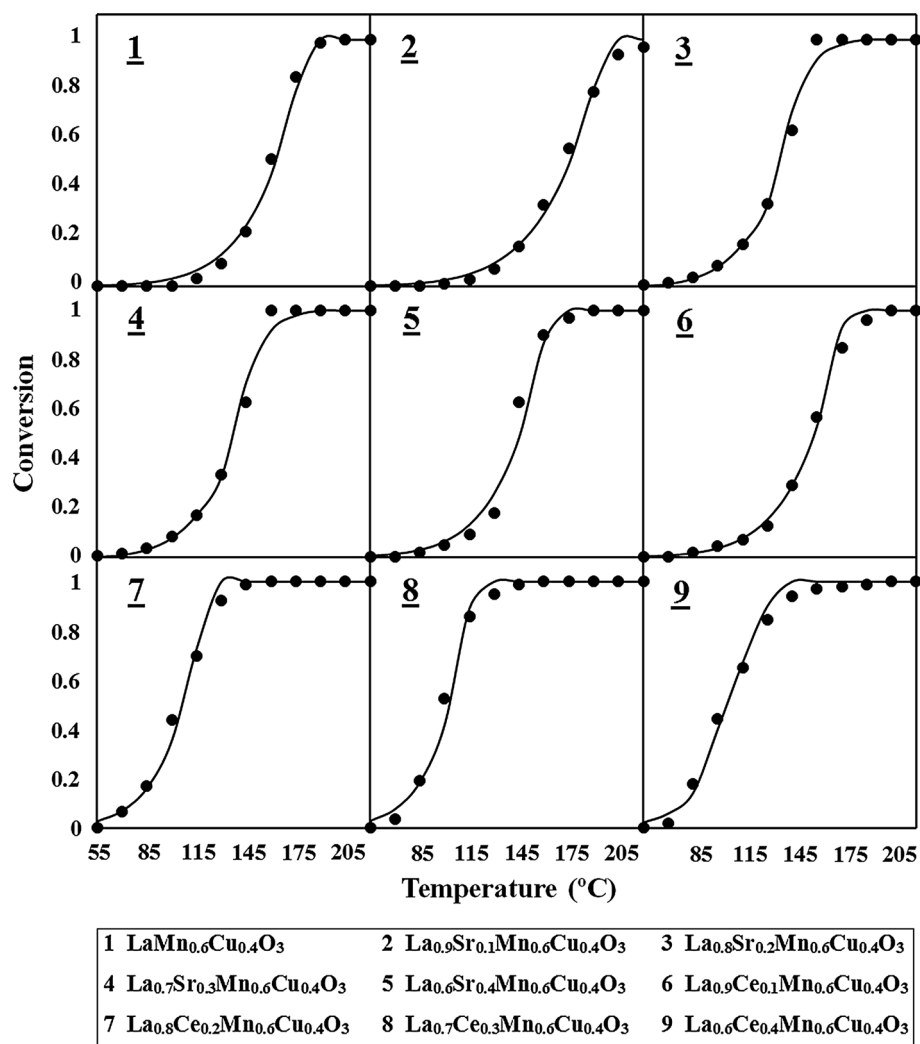


Fig. 6 Comparison between experimental and simulated data for Langmuir–Hinshelwood model, competitive adsorption on one single type of sites and non-dissociative adsorption of oxygen (LH–OS–ND); best fit (–), experimental (filled circles)

first mechanism [$CO + S \rightarrow (CO)S$; $O_2 + S \rightarrow (O_2)S$] is more possible than the other proposed mechanism. Based on the obtained results, following mechanisms should be considered to be possible: LH–OS–ND, LH–DS–ND, LH–OS–D, LH–DS–D. Comparisons between experimental and modeling results for CO conversion for LH–OS–ND models are shown in Fig. 6. The results of the fitting procedure for CO conversion for all catalysts in the range of reaction temperature (55–220 °C) for LH–OS–ND model are shown in Fig. 7. It is clear from Fig. 7 that there is a good agreement between experimental and calculated data.

Fig. 7 CO conversion in the range of reaction temperature (55–220 °C) for Langmuir–Hinshelwood model, competitive adsorption on one single type of sites and non-dissociative adsorption of oxygen (LH–OS–ND); experimental (filled circles), modeling (–)



The estimated values including k_0 , E_1 , $k_{0,\text{CO}}$, ΔH_{CO} , $k_{0,\text{OX}}$ and ΔH_{OX} for LH–OS–ND mechanism, R^2 and AAD% for all catalysts are also listed in Table 3. The values of E_1 do not show any tangible change with A' cation and x value and remain in the range $23 < E_{\text{app,low}} < 33$ (kJ/kmol). The pre-exponential factors for various catalysts are different. This can probably be explained by the presence of different metal and x values which can affect the performance of perovskite catalysts, leading to different amounts of pre-exponential factors for reaction rate.

Conclusion

Catalytic performance of $\text{La}_{1-x}\text{A}_x\text{Mn}_{0.6}\text{Cu}_{0.4}\text{O}_3$ ($\text{A} = \text{Sr}, \text{Ce}$, $x = 0, 0.1, 0.2, 0.3$ and 0.4) perovskite catalysts obtained by sol–gel auto-combustion method was evaluated for CO oxidation. Perovskite catalysts were

characterized by XRD, BET, FT-IR, H_2 -TPR and SEM. XRD results confirmed that pure perovskite crystal phases were obtained via sol–gel auto-combustion method. SEM results also revealed that morphology of perovskites is spherical and size of crystals is less than 100 nm. Complete elimination of CO was achieved under 150 °C with the studied catalysts. The reducibility of the synthesized perovskites is strongly affected by substitution of La by Sr and Ce. In addition, perovskite catalysts showed high activities for CO oxidation. Substitution of A site cation in perovskite catalysts led to strong modifications of their activities. Our results demonstrate that the perovskite mixed oxides are very promising materials as catalysts for CO oxidation with good performances. In order to conduct kinetic studies, kinetic parameters were obtained based on Langmuir isotherm. Four Langmuir–Hinshelwood mechanisms were investigated. Kinetic parameters including k_0 , E_1 , $k_{0,\text{CO}}$, ΔH_{CO} , $k_{0,\text{OX}}$ and ΔH_{OX} were estimated. High value of R^2 (>0.97) showed that the Langmuir–

Hinshelwood models can predict the experimental data with a good accuracy. According to the obtained results, kinetic study of CO oxidation over $\text{La}_{1-x}\text{A}_x\text{Mn}_{0.6}\text{Cu}_{0.4}\text{O}_3$ revealed that LH–OS–ND mechanism [$\text{CO} + \text{S} \rightarrow (\text{CO})\text{S}$; $\text{O}_2 + 2\text{S} \rightarrow (\text{O}_2)\text{S}$] was more possible than the other mechanisms. This study shows that the reported model can successfully be used for prediction of catalyst activity in CO oxidation.

Acknowledgments Financial supports from the Iran Nanotechnology Initiative Council (Grant No. 84870) are gratefully acknowledged.

References

- Abdolrahmani M, Parvari M, Habibpoor M (2010) Effect of copper substitution and preparation methods on the $\text{LaMnO}_{3\pm\delta}$ structure and catalysis of methane combustion and CO oxidation. *Chin J Catal* 31:394–403
- Ferrer V, Finol D, Solano R, Moronta A, Ramos M (2015) Reduction of NO by CO using Pd–CeTb and Pd–CeZr catalysts supported on SiO_2 and $\text{La}_2\text{O}_3\text{--Al}_2\text{O}_3$. *J Environ Sci* 27:87–96
- Gao B, Deng J, Liu Y, Zhao Z, Li X, Wang Y, Dai H (2013) Mesoporous LaFeO_3 catalysts for the oxidation of toluene and carbon monoxide. *Chin J Catal* 34:2223–2229
- Gupta V, Agarwal S, Saleh TA (2011a) Chromium removal by combining the magnetic properties of iron oxide with adsorption properties of carbon nanotubes. *Water Res* 45:2207–2212
- Gupta V, Gupta B, Rastogi A, Agarwal S, Nayak A (2011b) Pesticides removal from waste water by activated carbon prepared from waste rubber tire. *Water Res* 45:4047–4055
- Gupta VK, Agarwal S, Saleh TA (2011c) Synthesis and characterization of alumina-coated carbon nanotubes and their application for lead removal. *J Hazard Mater* 185:17–23
- Gupta VK, Jain R, Saleh T, Nayak A, Malathi S, Agarwal S (2011d) Equilibrium and thermodynamic studies on the removal and recovery of safranin-T dye from industrial effluents. *Sep Sci Technol* 46:839–846
- Gupta VK, Jain R, Mittal A, Saleh TA, Nayak A, Agarwal S, Sikarwar S (2012) Photo-catalytic degradation of toxic dye amaranth on TiO_2/UV in aqueous suspensions. *Mater Sci Eng C* 32:12–17
- Harriott P (2002) *Chemical reactor design*. CRC Press, London
- Hosseini SA, Sadeghi MT, Alemi A, Niaei A, Salari D, Leila K-A (2010) Synthesis, characterization, and performance of $\text{LaZn}_x\text{Fe}_{1-x}\text{O}_3$ perovskite nanocatalysts for toluene combustion. *Chin J Catal* 31:747–750
- Hosseini SA, Salari D, Niaei A, Oskoui SA (2013) Physical–chemical property and activity evaluation of $\text{LaB}_{0.5}\text{Co}_{0.5}\text{O}_3$ (B = Cr, Mn, Cu) and $\text{LaMn}_x\text{Co}_{1-x}\text{O}_3$ ($x = 0.1, 0.25, 0.5$) nano perovskites in VOC combustion. *J Ind Eng Chem* 19:1903–1909
- Jaenicke S, Chuah G, Lee J (1991) Catalytic CO oxidation over manganese-containing perovskites. In: Kee Lee H (ed) *Fourth symposium on our environment*. Springer, Berlin, pp 131–138
- Karthikeyan S, Gupta V, Boopathy R, Titus A, Sekaran G (2012) A new approach for the degradation of high concentration of aromatic amine by heterocatalytic Fenton oxidation: kinetic and spectroscopic studies. *J Mol Liq* 173:153–163
- Khanfekr A, Arzani K, Nemati A, Hosseini M (2009) Production of perovskite catalysts on ceramic monoliths with nanoparticles for dual fuel system automobiles. *Int J Environ Sci Technol* 6:105–112
- Ladas S, Poppa H, Boudart M (1981) The adsorption and catalytic oxidation of carbon monoxide on evaporated palladium particles. *Surf Sci* 102:151–171
- Libby W (1971) Promising catalyst for auto exhaust. *Science* (New York, NY) 171:499–500
- Lin Y-C, Hohn KL (2014) Perovskite catalysts—a special issue on versatile oxide catalysts. *Catalysts* 4:305–306
- Megha U, Shijina K, Varghese G (2014) Nanosized $\text{LaCo}_{0.6}\text{Fe}_{0.4}\text{O}_3$ perovskites synthesized by citrate sol gel auto combustion method. *Process Appl Ceram* 8:87–92
- Meiqing S, Zhen Z, Jiahao C, Yugeng S, Jun W, Xinquan W (2013) Effects of calcium substitute in LaMnO_3 perovskites for NO catalytic oxidation. *J Rare Earths* 31:119–123
- Patel F, Patel S (2013) $\text{La}_{1-x}\text{Sr}_x\text{CoO}_3$ ($x = 0, 0.2$) perovskites type catalyst for carbon monoxide emission control from auto-exhaust. *Proc Eng* 51:324–329
- Pena M, Fierro J (2001) Chemical structures and performance of perovskite oxides. *Chem Rev* 101:1981–2018
- Piccolo L, Becker C, Henry C (1999) Kinetic modeling of the CO oxidation reaction on supported metal clusters. *Eur Phys J D Atomic Mol Opt Plasma Phys* 9:415–419
- Saleh TA (2016) Nanocomposite of carbon nanotubes/silica nanoparticles and their use for adsorption of Pb(II): from surface properties to sorption mechanism. *Desalination Water Treat* 57:10730–10744
- Saleh TA, Gupta VK (2011) Functionalization of tungsten oxide into MWCNT and its application for sunlight-induced degradation of rhodamine B. *J Colloid Interface Sci* 362:337–344
- Saleh TA, Gupta VK (2012) Photo-catalyzed degradation of hazardous dye methyl orange by use of a composite catalyst consisting of multi-walled carbon nanotubes and titanium dioxide. *J Colloid Interface Sci* 371:101–106
- Saleh TA, Agarwal S, Gupta VK (2011) Synthesis of MWCNT/ MnO_2 and their application for simultaneous oxidation of arsenite and sorption of arsenate. *Appl Catal B* 106:46–53
- Singh UG, Li J, Bennett JW, Rappe AM, Seshadri R, Scott SL (2007) A Pd-doped perovskite catalyst, $\text{BaCe}_{1-x}\text{PdxO}_{3-\delta}$, for CO oxidation. *J Catal* 249:349–358
- Tanaka H, Misono M (2001) Advances in designing perovskite catalysts. *Curr Opin Solid State Mater Sci* 5:381–387
- Tarjomannejad A (2015) Prediction of the liquid vapor pressure using the artificial neural network-group contribution method. *Iran J Chem Chem Eng* 34:97–111
- Vannice MA, Joyce WH (2005) *Kinetics of catalytic reactions*. Springer, Berlin
- Voorhoeve R, Johnson D, Remeika J, Gallagher P (1977) Perovskite oxides: materials science in catalysis. *Science* 195:827–833
- Wagloehner S, Reichert D, Leon-Sorzano D, Balle P, Geiger B, Kureti S (2008) Kinetic modeling of the oxidation of CO on Fe_2O_3 catalyst in excess of O_2 . *J Catal* 260:305–314
- Wang K, Zhong P (2010) A kinetic study of CO oxidation over the perovskite-like oxide LaSrNiO_4 . *J Serb Chem Soc* 75:249–258
- Xu X, Szanyi J, Xu Q, Goodman DW (1994) Structural and catalytic properties of model silica-supported palladium catalysts: a comparison to single crystal surfaces. *Catal Today* 21:57–69



- Yan X, Huang Q, Li B, Xu X, Chen Y, Zhu S, Shen S (2013) Catalytic performance of $\text{LaCo}_{0.5}\text{M}_{0.5}\text{O}_3$ ($M = \text{Mn, Cr, Fe, Ni, Cu}$) perovskite-type oxides and $\text{LaCo}_{0.5}\text{Mn}_{0.5}\text{O}_3$ supported on cordierite for CO oxidation. *J Ind Eng Chem* 19:561–565
- Yoon JS, Lim Y-S, Choi BH, Hwang HJ (2014) Catalytic activity of perovskite-type doped $\text{La}_{0.08}\text{Sr}_{0.92}\text{Ti}_{1-x}\text{M}_x\text{O}_{3-\delta}$ ($M = \text{Mn, Fe, and Co}$) oxides for methane oxidation. *Int J Hydrog Energy* 39:7955–7962

